THERMAL ANNEALING OF SOLID Kr PRECIPITATES IN Ni*

R. C. BIRTCHER**, J. REST***, AND D. S. BERGSTROM**
**Materials Science Division, ***Materials and Components Technology Division
Argonne National Laboratory
Argonne, IL 60439

CONF-891119--57

DE90 004885

November 1989

Presented at the MRS 1989 Fall Meeting, Symposium A: Beam-Solid Interactions: Physical Phenomena", November 27-December 2, 1989, Boston, MA.

*Work supported by the U. S. Department of Energy, BES-Materials Sciences, under Contract W-31-109-Eng-38.

THERMAL ANNEALING OF SOLID Kr PRECIPITATES IN Ni*

R. C. BIRTCHER**, J. REST***, AND D. S. BERGSTROM**
**Materials Science Division, ***Materials and Components Technology Division, Argonne National Laboratory, Argonne, IL 60439, USA

ABSTRACT

After implantation into Ni at room temperature, Kr condenses under high pressure as an fcc solid aligned with the Ni lattice. Evolution of these precipitates during subsequent thermal annealing to a temperature of 650 C has been followed with transmission electron microscopy and modeled with rate theory.

Room temperature implantation results in a monomodal size distribution of small solid Kr precipitates. When Kr is implanted into Ni at 500 C, some precipitates grow to larger sizes, and the precipitate size distribution becomes bimodal. Annealing to temperatures below 600 C after room temperature implantation produces a bimodal size distribution consisting of small solid Kr precipitates and large Kr bubbles. Annealing above 600 C leads to more complete precipitate motion and coalescence that eliminates all small precipitates and results in a monomodal size distribution of large faceted bubbles.

Rate-theory modelling of Kr implantation into Ni at 500 C suggests that small solid Kr precipitates are immobile and that Kr melting is required for precipitate mobility. Similar calculations for thermal annealing experiments show that the bubble size distribution becomes bimodal when only a small fraction of the small precipitates melt and become mobile during annealing, while the size distribution remains monomodal when all precipitates become mobile after Kr melting at higher temperatures.

INTRODUCTION

Rare gas ions inadvertently implanted during their use in surface modification or ion beam mixing may reach atom concentrations of several percent. At such levels, the insoluble rare gases precipitate into small cavities. The evolution of the rare-gas precipitates during implantation or subsequent thermal annealing can have a major impact on material properties. The results of several studies show that in general the heavy rare-gases (Ne, Ar, Kr, Xe) will precipitate in cavities under high pressures as liquids or as crystalline solids aligned with the host material [1,2,3,4,5]. The concentration dependence of Kr precipitation has been investigated in detail for Ni implanted at temperatures between 30 C and 560 C [4,5]. Kr precipitates increase in size with Kr fluence. Precipitates are under high pressures, and those with radii less than about 3 nm are solid, fcc crystals epitaxically aligned with the Ni lattice. Liquid precipitates freeze on cooling, and solid precipitates melt upon heating. Melting temperatures decrease with increasing precipitate size (lower pressure).

In this study, Kr precipitates were formed by room temperature implantation into Ni thin films and studied by TEM during in situ thermal annealing. TEM bright-field images have been used to determine the evolution the microstructure with Kr fluence, and electron diffraction and dark-field imaging

*Work supported by the U. S. DOE, Basic Energy Sciences-Materials Sciences under Contract #W-31-109-ENG-38.

have been used to investigate the solidification and epitaxy of Kr precipitates. Average Kr lattice parameters were determined from electron diffraction patterns. The experimental results were modeled using a rate theory to investigate the importance of atomic Kr, defect and precipitate mobility.

EXPERIMENTAL PROCEDURES

Thin single-crystal Ni films (70 nm thick) were prepared by evaporation of high purity Ni in a vacuum less than $1 \cdot 10^{-7}$ Torr onto freshly cleaved NaCl at a temperature of 350 C. The coated NaCl was cleaved into small pieces, and specimens were floated on a water-methanol mixture onto Cu TEM grids. Implantations were performed with 180 keV Kr^+ ions at fluxes less than $2 \cdot 10^{16}$ $Kr^+m^{-2}sec^{-1}$. During implantation, the TEM grids were clamped at their periphery against a Cu disk. The implantation energy was selected on the basis of the results from the TRIM computer code [6]. AT 180 keV, the Kr concentration depth profile within the Ni films has it maximum near the foil center and decreases to near zero at both foil surfaces. Estimates for a fluence of $1 \cdot 10^{20}$ Kr^+m^{-2} yield a damage level of 33 displacements per atom at the location of the peak in the Kr concentration of 3.14 % . Sputtering for this fluence will cause the depth peaks to shift nearer the back surface of the specimen by 11 nm (or less due to the surface oxide) [7].

Post-implantation TEM observations were made with a JEOL JEM-100-CX at an operating voltage of 100 keV and at magnifications up to 100,000. Details within the specimens greater that 1 nm were detectable. The Kr precipitates were imaged in bright field by their defocus contrast. Electron diffraction patterns were generated with the electron beam parallel to the <100> specimen normal, and the average solid-Kr lattice parameter was determined from the positions on the micrograph of intensity maxima due to Kr and Ni {200} reflections. The solid Kr precipitates were imaged in dark field from electrons scattered into a Kr {200} reflection. In situ elevated-temperature observations were made with a Gatan heating stage, however, specimen oxidation restricted the observations to temperatures about 650 C. Images were recorded at increasing temperatures after the specimen holder had equalibrated and the specimen position was stable. At most temperatures, this required about 10 minutes.

Calculational Procedures

The behavior of Kr atoms in Ni during both implantation and thermal annealing has been modeled with a rate theory approach [8,9,10] that approximates the bubble-size distribution by grouping bubbles into size classes, each characterized by a fixed number of Kr atoms, and includes mechanisms such as bubble nucleation, migration and coalescence. The equations have the form:

$$\frac{dC_i}{dt} = -A_iC_iC_i - B_iC_i + F_i \,, \qquad (1)$$

where C_i is the number of bubbles in the i^{th} class per unit volume, A_i represents the rate at which bubbles are lost from the i^{th} class due to coalescence with bubbles in that class, B_i represents the rate at which bubbles are lost from the i^{th} class due to coalescence with bubbles in any other class, and F_i represents the rate at which bubbles are added to the i^{th} class due to coalescence and Kr

precipitation. The A_i's are independent of the C_i's while B_i and F_i depend on all C_j's except for j=i. Neglecting bubble over pressurization effects, the rate of precipitation into the i^{th} bubble class is given by:

$$F_i^P = 4\pi(r_a + r_i)(D_a + D_i)(C_a - C_a^o), \quad (2)$$

where r_a is the radius of a gas atom, r_i is the average radius of bubbles in the i^{th} class, D_a is the Kr diffusion coefficient, D_i is the diffusion coefficient of bubbles in the i^{th} class, C_a is the Kr concentration in solution, and C_a^o is the Kr atom solubility. Precipitation into over pressurized bubbles will be reduced by the surrounding elastic strain field [11,12]. To account for this effect, Equation (2) should be multiplied by a exponential whose argument is $(-\Delta g_i/R_g)$, where Δg_i is the energy of interaction between a gas atom and the i^{th} bubble strain field, R_g is the gas constant, and T is the absolute temperature.

Previous studies of rare gas implantation in metals [9,10] presented strong evidence that the basic bubble migration mechanism is non-localized surface diffusion limited by the interaction between the diffusing surface defect and gas atoms in the bubble. The strong interaction expected between surface defects and solid Kr precipitates drastically reduces solid precipitate mobility. In the model, this mobility is reduced to zero. Precipitate melting at high temperature allows bubble mobility leading to bubble coalescence and growth. These effects have been included in equations 1 and 2.

Experimental Results and Discussion

Ni was implanted at room temperature with 180 KeV Kr. Detailed studies [4,5] of the temperature dependence of Kr precipitation in Ni has shown that at room temperature rare gas precipitation in Ni is driven by the Kr concentration and not atomic mobilities. This results in a monomodal precipitate size distribution containing small precipitates (radius<3nm). With increasing dose, precipitates grow by accumulating Kr atoms and their associated vacancies. Kr in such precipitates is under a high pressure that hold the atoms in the solid phase. Kr precipitates formed during implantation at temperatures above 450 C evolve from a monomodal size distribution of small precipitates at low doses, similar to room temperature size distributions, to a bimodal distribution containing additional large faceted precipitates [4,5]. Formation of large precipitates is preceded by solid Kr melting in growing small precipitates. Solid Kr prevents surface diffusion, and thus precipitate migration. Faceting is controlled by the surface energy, and (100) and (111) atomic planes are the dominate planes observed.

Thermal annealing results in increased motion of atoms and Kr precipitates. Figure 1 shows TEM images taken during thermal annealing to 650 C of a specimen initially implanted at room temperature to a dose of $4 \cdot 10^{20}$ Kr^+m^{-2}. There was little change in the Kr precipitates during annealing at temperatures below 550 C. Above this temperature all solid Kr precipitates melted. Visible precipitate growth began during heating to 590 C, and additional growth occurred slowly during continued annealing at 590 C. A dramatic increase in the precipitate sizes occurred on heating to 650 C. At this temperature, small precipitates were observed to migrate. This movement results in precipitate coalescence and a rapid growth of the precipitates into gas bubbles. Bubbles grew to very large sizes at which they are nearly immobile. The events leading to the formation of any particular large bubble could be easily followed during

annealing. The sequence involves small bubble migration, growth by coalescence, necking between large nearly immobile bubbles, and rounding-out of irregularly shaped necked bubbles. Additional coalescence and necking between nearly immobile large bubbles occurred when the rounding-out process resulted in their close approach. This lead to runaway precipitate growth. Very large bubbles occasionally intersected the specimen surface. When this occurred, the resulting steps on the specimen surface rapidly migrated away from the site of the bubble. Rapid bubble growth finally leaded to failure of the thin film specimen.

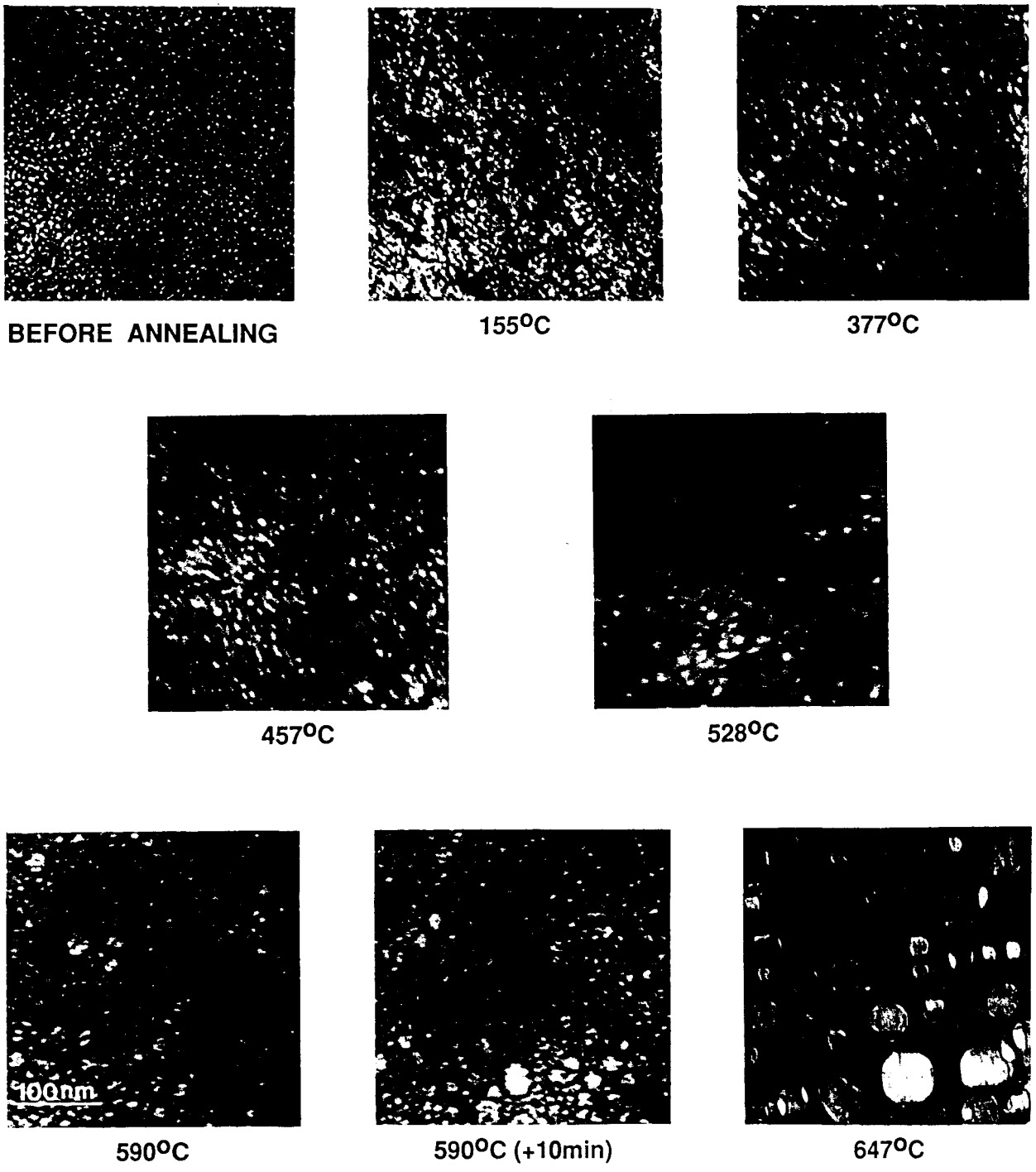

Figure 1 TEM images taken during warm-up to 650 C of Ni containing $4 \cdot 10^{20}$ $Kr^{+}m^{-2}$.

Modelling Results

This section discusses the results of calculations of precipitate behavior during thermal annealing that follow calculation of precipitate formation during implantation [9,10]. Figure 2 shows the time evolution of Kr precipitates in Ni, $4 \cdot 10^{20}$ $Kr^{+}m^{-2}$, during annealing at 500 C. During warm up to 500 C at a rate of 10 C/s, the size distribution remains monomodal with the peak occurring at about 15 Å radius. With increasing time at 500 C, the size distribution becomes bimodal. The peak at smaller sizes consist of immobile solid Kr precipitates while the peak at larger sizes consist of non-solid Kr bubbles that are capable of motion by surface diffusion. Initially the solid precipitates grow by Kr absorption due to increased Kr atom mobility. After growth to non-solid sizes (radius > 20Å), bubbles become mobile, and coalescence leads to a decrease in the number density of small precipitates and an increase in the average size of larger non-solid bubbles.

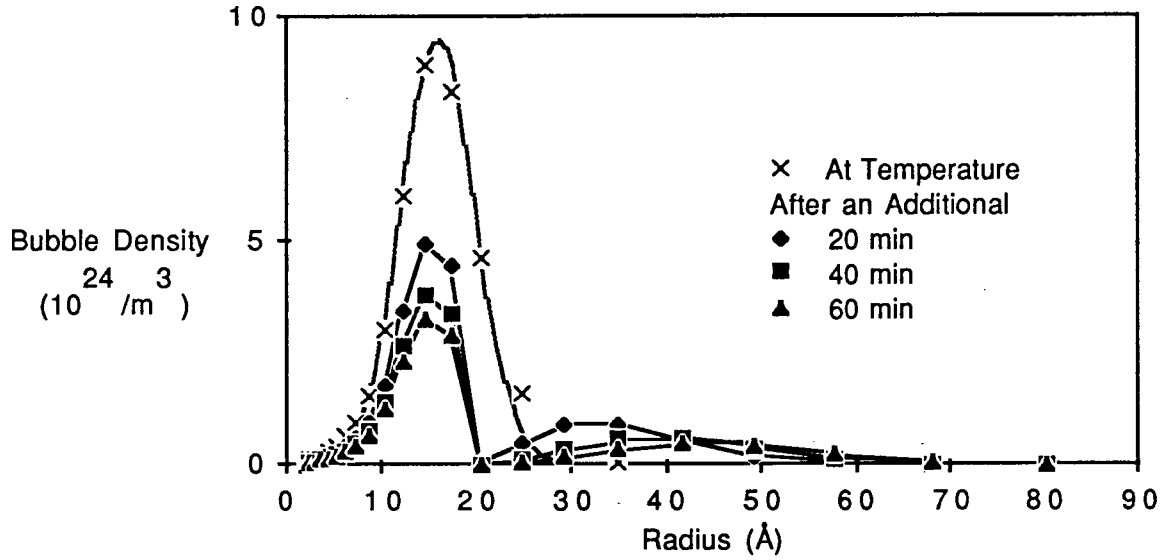

Figure 2. Calculated time variation of the Kr bubble size during annealing at 500 C after warm-up at 10K/s.

The rate of small precipitate growth is limited by the amount of Kr in solution, and large bubble growth is mitigated by decrease of bubble mobility with increasing size. The size distribution becomes bimodal because of the lack of small bubble motion and restriction of bubble coalescence to the immediate vicinity of mobile large bubbles.

When a specimen is annealed directly to 650 C at 10 C/s, thermodynamic Kr melting occurs in all bubbles, and small precipitates become mobile without additional Kr accumulation and growth. The results of calculations are shown in Figure 3. The curves in Figure 3 are Gaussian fits to the data. At 650 C, sudden migration of all small bubbles results in coalescence amongst all small bubbles and a rapid shift of the monomodal size distribution to large sizes.

Conclusions

The modeling results are in agreement with our experimental observations. The calculations suggest that the relative low experimental heating rate did not produce over pressurized bubbles. The growth of Kr precipitates during high dose rate implantation is "gas driven" as compared to "bias driven", and solid Kr precipitates are immobile. Kr melting,induced by precipitate growth or temperature, allows bubble migration by surface diffusion.

During thermal annealing after room temperature implantation, the bubble size distribution becomes bimodal when only a relative small fraction of the bubbles are mobile, while it remains monomodal if all bubbles become mobile and participate in coalescence.

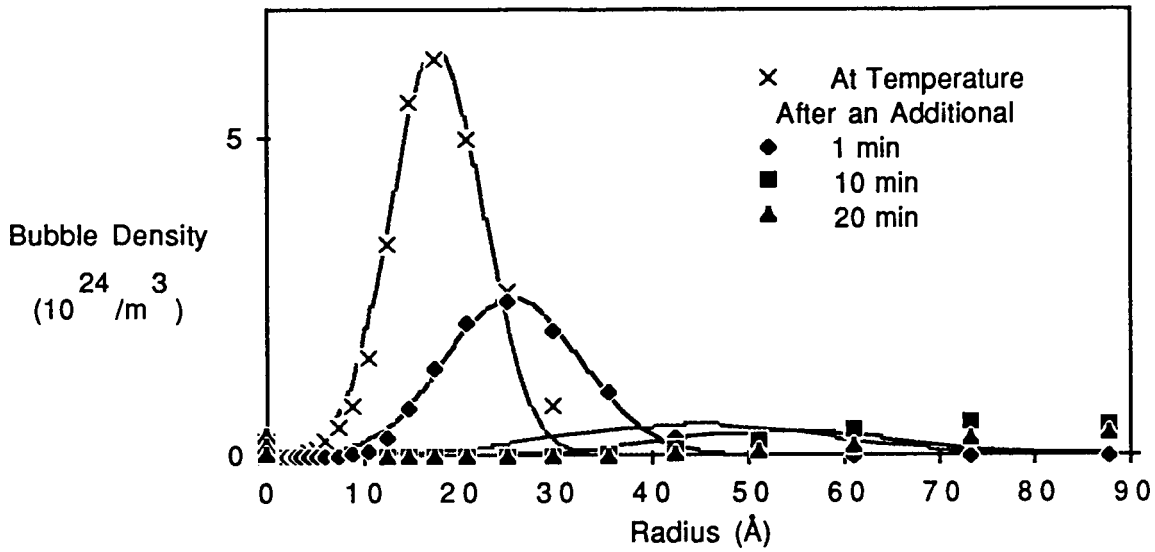

Figure 3. Calculated time variation of the Kr bubble size during annealing at 650 C after warm-up at 10K/s.

References

[1] A. vom Felde, J. Fink, Th. Müller-Heinzerling, J. Pflüger, B. Scheerer and G. Linker, Phys. Rev. Lett. 53 ,922 (1984).

[2] J. H. Evans and D. J. Mazey, J. Phys. F:Met.Phys.15,L1 (1985).

[3] R. C. Birtcher and W. Jäger, Ultramicroscopy, 22, 267 (1987).

[4] R. C. Birtcher and A. S. Liu, in Beam-Solid Interactions and Transient Processes, edited by M.O. Thompson, S.T. Picraux and J.S. Williams (Mater. Res. Soc. Proc. 74, Boston, Ma. 1986) pp. 345-350.

[5] R. C. Birtcher and A. S. Liu, J. Nucl. Mater 165, 101 (1989).

[6] J. Biersack and L. G. Haggmark, Nucl. Instr. and Meth. 174, 257 (1980).

[7] H. H. Andersen and H. L. Bay, in Sputtering by Particle Bombardment, I, R. Behrisch ed. Topic Appl. Phys., vol.47 (Springer, Berlin 1981), page 145.

[8] J. Rest, "GRASS-SST: A Comprehensive, Mechanistic Model for the Prediction of Fission-Gas Behavior in UO_2-Base Fuels During Steady-State and Transient Conditions", NUREG/CR-0202, Argonne National Laboratory Report ANL-78-53 (1978).

[9] J. Rest and R. C. Birtcher, 14 Int. Symp. Effects Radiat. on Mater., June 27 -29,1988, Andover, Ma, USA.

[10] R. C. Birtcher and J. Rest, J. Nucl. Mater, to be published.

[11] C. Ronchi, J. Nucl. Mater, 148,316 (1987).

[12] J. Rest, J. Nucl. Mater, to be published.